Results in Physics 13 (2019) 102310

Contents lists available at ScienceDirect

Results in Physics

journal homepage: www.elsevier.com/locate/rinp

Simulation and experimental measurement of digital multi-beamforming phased antenna array in the frequency range C

Lu Guoming[a,*], Fairuza M. Sabirova[b], Alexander V. Morozov[c]

[a] Faculty of Physics, Lomonosov Moscow State University, GSP-1, 1-2 Leninskiye Gory, Moscow 119991, Russian Federation
[b] Department of Physics, Elabuga Institute of Kazan Federal University, 89 Kazan Str., Elabuga 423600, Republic of Tatarstan, Russian Federation
[c] Department of Geology of Oil and Gas Fields, Tyumen Industrial University, 56 Volodarsky Str., Tyumen 625000, Russian Federation

ARTICLE INFO

Keywords:
Phased array antenna
Radiation pattern
Digital beamforming
Standing wave voltage ratio

ABSTRACT

The selection of element for constructing a phased array antenna was carried out. It provides a relative frequency bandwidth up to 9% for the transmitting or receiving part in wireless communication system. Methods of reducing the sidelobe for the far field pattern are compared and analyzed. The superposition of excitation signals for a flat phased array antenna was implemented to simultaneously generate the emission of independent beams in a far radiation field. The calculation and optimization of progressive distribution was performed for phase shifts in the excitation signal group from the horizontal and vertical directions of the phased array plane for a radiation (reception) of independent beams in space. An experimental sample of a digital phased array antenna was developed using microstrip technology. A novel digital feeding method is proposed and employed in Multiple Input Multiple Output (MIMO) communications system. An experimental measurement was carried out in term of the voltage standing wave ratio, the relative frequency bandwidth and the radiation pattern of sample from digital beamforming technology.

Introduction

In modern communication systems a large data throughput is highly desirable in [1,2]. The extension from bandwidth and transmission power are limited, and in many cases do not allow providing the required throughput [3]. A diversity receiving and transmitting MIMO Communication systems provides an additional opportunity to increase the data throughput [2,4]. In most cases MIMO systems use several antennas or multi-element antennas for transmitting and receiving [2,4]. Digital multi-beam phased array antenna (PAA) is the one of the way of organizing the MIMO channel [5,6]. Multipath propagation of radio waves can be used to improve the energy and spectral transmission efficiency [7]. Multipath propagation of radio waves is typical for urban environments and radio channels inside buildings. It provides an opportunity to transfer energy along several spatial trajectories. In multiple access systems different directions of transmission and reception can be used to communicate with different subscribers in order to increase the total throughput of the system [8–10]. Multipath radiation pattern for wideband and ultra-wideband PAA can be formed with both analog and digital methods [4,11,12]. In analog methods, a feeder system, a set of phase shifters and summators on antenna ports are used according to the rule. The complexity of this construction increases significantly as the increasing number of beams and elements of PAA. Such schemes can be used to form less than 2–3 beams [4]. A digital circuit of the formation for a multipath radiation pattern provides a number of advantages [4,10,11,13,14]:

- the possibility of dynamic high-speed change for the beam shape; compatibility with modern effective means of digital signal processing technique; the shape and direction of beam provided by the programming;
- the possibility the possibility of targeting the partial beams on individual users or their spatially-focused group that ensures maximum performance of all communication channels;
- the permission to control and compensate any spurious changes in the amplitude and phase of signals along the propagation path between transmitter and receiver;
- the possibility of far software reconfiguration of architecture, the modernization of signals processing methods and modes of the system operation;
- the permission to the digital beamforming for implementing the efficient dynamic adaptation of the service coverage area over ground cells [11].

* Corresponding author.
E-mail address: luguoming.hit@gmail.com (L. Guoming).

https://doi.org/10.1016/j.rinp.2019.102310
Received 6 September 2018; Received in revised form 17 April 2019; Accepted 22 April 2019
Available online 26 April 2019

The microstrip antenna was chosen due to its advantages of low thickness, enabling to placing the antennas together on a printed circuit board, and compatibility with modern effective methods of digital circuits [2,4,15]. The study was carried out with the help of simulation in the software package CST Microwave Studio, which uses the time-domain finite integral due to its advantages of only one pulse in the time domain being able to cover a wide frequency band [16]. The Chebyshev current distribution on the elements for synthesis of antenna arrays with a given number of sidelobes and sidelobe levels is discussed in [17,18]. The Gegenbauer polynomials are used to synthesis pattern of array antennas which have high directivity and low sidelobe level [19]. The syntheses polygonal arrays with prescribed pattern nulls are implemented in [20]. For the synthesis of the series-fed microstrip array antenna, the microstrip power dividers and phase shifters are used in [21]. This paper presents a new digital feed method for generating the beam.

The structure of this article is as follows: the first part describes the choice of the element of PAA, which provides a relative frequency band up to 9% at a central frequency of 7 GHz; the second part deals with the comparison of methods for suppressing side lobes; the third part gives a simulation of a flat microstrip PAA with an emitting beams; the fourth and fifth parts present the results of experimental measurements of PAA.

Material and methods

The frequency bandwidth of the microstrip antenna depends on many parameters: the geometric shape of the patch element, the dielectric permittivity of the substrate and the thickness of the substrate material. The frequency bandwidth increases with the growth of the thickness of the dielectric substrate and decreases with the growth of the dielectric permeability of the substrate material. In view of this, the dielectric material (Arlon AD255, $\varepsilon = 2.55$, $h = 2.032$ mm) was chosen with a low dielectric permeability and a high dielectric substrate thickness.

In order to study the dependence of the frequency bandwidth on the geometric shape of the patch element and the choice of broadband elements, a simulation for elements in different shapes was carried out. It includes the rectangular, the rectangular with rounded corners, the fan shape, the fan shape with rounded corners, the butterfly shape with rounded corners, circle, and hexagon. The simulation results are presented in Table 1.

The following parameters were used in the calculation and simulation: a central frequency of 7 GHz, a substrate material of Arlon AD255 (with dielectric permeability $\varepsilon = 2.55$ and thickness $h = 2.032$ mm) and a thickness of the copper patch 18 μm. The simulation results show that the rectangular patch with rounded corners provides the widest bandwidth among the studied forms. In view of this, the rectangular patch with rounded corners was chosen as the main element for constructing arrays. The simulation results of the radiation pattern and VSWR of the selected element shows a gain of 7 dBi at the operating frequency band of 6.7–7.3 GHz with the central frequency at 7 GHz. A size of the antenna patch is 16×12.8 mm. The schematic antenna element, simulation results of the S-parameters (S11) and the radiation pattern are shown in Fig. 1.

Results and discussion

Suppression of the level of PAA side lobes

In order to reduce the side lobes of the radiation pattern in the far field of the antenna array, the following methods are used [22]:

(a) reducing distances between elements into the values less than $\lambda/2$;
(b) non-equidistant arrangement of elements;
(c) uneven distribution of currents on the elements;
(d) the use of highly directional elements.

Unfortunately, the work [22] does not give further information about the efficiency under the aforementioned all methods. The methods (d) is suitable for highly directional element and is not suitable for the selected element in this article. The further investigation and comparison are required in terms of methods (a), (b) and (c). The antenna array will be constructed using the selected patch in both horizontal and vertical directions on the plane. The antenna element position distribution is shown in Fig. 2. In order to reduce the Side Lobe Level (SLL), the horizontal and vertical elements spacing (dx and dy) should be optimized.

Location of PAA elements at a distance of less than λ/2

At the equal distance between the elements $d > \lambda/2$, the far radiation field may contain several side lobes which have the relatively same level with the main lobe [22]. During the method of reducing side lobes (including diffraction), the reduction of the distance between the elements is less $\lambda/2$. The simulation at $d < \lambda/2$ is carried out. A study for the SLL of 6-element PAA is investigated at horizontal line with $dx1 = dx2 = dx3 = dx4 = dx5 = dx < \lambda/2$ and a radiation in directions of 30°, 45° and 60° from the normal direction. For vertical line PAA, a study of $dy1 = dy2 = dy3 = dy4 = dy5 = dy < \lambda/2$ with the radiation in directions of 30°, 45° and 60° from the normal direction was realized. The simulation results are presented in Table 2.

Based on the simulation results of linear PAA in both horizontal and vertical directions for a calculated elements spacing of less than $\lambda/2$, a significant suppression of the side lobe (including diffraction) in the far field radiation less than −12 dB is achieved. At the distance of elements spacing at $0.47\lambda = 20$ mm, the side lobe has a maximum suppression.

Non-equidistant arrangement of elements

In order to investigate the possibility of suppressing SLL by positioning the elements at unequal distances the model of the linear non-equidistant 6-element PAA was established; the normalized coordinates of the elements were obtained with calculation: $\xi_0 = -0.9994$, $\xi_1 = -0.5343$, $\xi_2 = -0.1705$, $\xi_3 = 0.1713$, $\xi_4 = 0.5352$ and $\xi_5 = 1$ [22]. The distance between the elements, respectively is relative to the

Table 1
Bandwidth for different geometric shapes of elements.

Element	Lower frequency (GHz)	Upper frequency (GHz)	Relative bandwidth (%)	Gain (dBi)
Rectangular	6.75	7.28	7.4	7.2
Rectangular with rounded corners	6.72	7.3	8.3	7.0
Fan	6.77	7.23	6.5	6.2
Fan with rounded corners	6.82	7.2	5.4	6.4
Butterfly	6.86	7.22	5.1	6.9
Butterfly with rounded corners	6.88	7.23	5.0	7.1
Hexagon	6.86	7.13	4.0	5.2
Circle	6.66	7.16	7.1	5.1

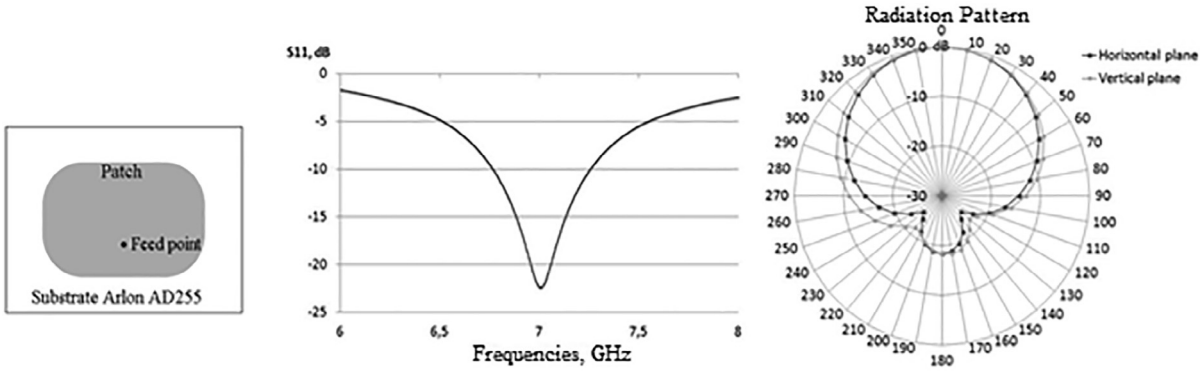

Fig. 1. S11-parameters and radiation pattern of antenna element.

coordinates ξ_0, ξ_1, ξ_2, ξ_3, ξ_4 and ξ_5 [22]. In method (a) the distance between the two elements is 0.47 λ, the side lobe level is with a minimum value of −12 dB in the horizontal and vertical directions. In view of this, 0.47λ was chosen as the central distance (the distance between ξ_2 and ξ_3) between the elements. Simulation of non-equidistant 6-element PAA is carried out to study SLL. For the horizontal 6-element PAA, a central distance of dx3 = 0.47λ is selected and it satisfies the relationship $dxi/dx3 = (\xi_i - \xi_{i-1})/(\xi_3 - \xi_2)$, where i = 1,2,3,4,5,6. Therefore, a value of dx1 = 27.22 mm, dx2 = 21.28 mm, dx4 = 21.29 mm and dx5 = 27.19 mm is obtained by calculations. Similarly, for the vertical 6-element PAA at central distance of dy3 = 0.47λ, the value of dy1 = 27.22 mm, dy2 = 21.28 mm, dy4 = 21.29 mm and dy5 = 27.19 mm is obtained. Radiation in directions of 30°, 45° and 60° from the normal direction was studied.

According to the simulation results of non-equidistant linear PAA in the horizontal and vertical directions, a significant suppression for the side lobe (including diffraction) in the far field radiation is with a minimum of −12.8 dB. However; the number of side lobes is much larger. For the non-equidistant linear PAA in horizontal direction, the level of the main radiation in the direction of 60° has a comparable value to the level of the side lobe. The simulation results are presented in Table 3.

Table 2
The SLL of PAA with a spacing of less than λ/2 (dB).

Horizontal linear PAA						
Directions	dx					
	SLL (dB)					
	0.376 λ	0.379 λ	0.385 λ	0.397 λ	0.42 λ	0.47 λ
30°	−11	−11.1	−11.3	−11.5	−11.5	−11.5
45°	−8.5	−8.9	−9.3	−9.9	−10.3	−9.9
60°	−2.8	−3.7	−4.2	−5	−5.6	−6.4
Vertical linear PAA						
Directions	dy					
	SLL (dB)					
	0.376 λ	0.379 λ	0.385 λ	0.397 λ	0.42 λ	0.47 λ
30°	−11.5	−11	−11.2	−11.7	−11.8	−12
45°	−9.9	−11.7	−11.3	−11.3	−10.5	−10.
60°	−6.4	−7.9	−8.3	−8.2	−8.4	−8

Uneven distribution of currents on the elements

To suppress the side lobes of the antenna array radiation pattern, there is still an important method: uneven distribution of currents on the elements [17,22,23]. In this method Chebyshev distribution was used. According to the above discussion results methods (a) and (b) do not significantly suppress the SLL. For the linear equidistant PAA, at distance of elements spacing of d = 0.47λ the maximum suppression of side slobes is up to −12 dB. In view of this, in the simulation and calculation of the side lobe level, d = 0.47λ was chosen to create a linear PAA with Chebyshev current distribution on the elements. According to Chebyshev polynomials function for a linear array with 4 elements and 6 elements the amplitude distribution of the current on the elements is 1:3:3:1 and 1:4:6:4:1 respectively [17,18]. The

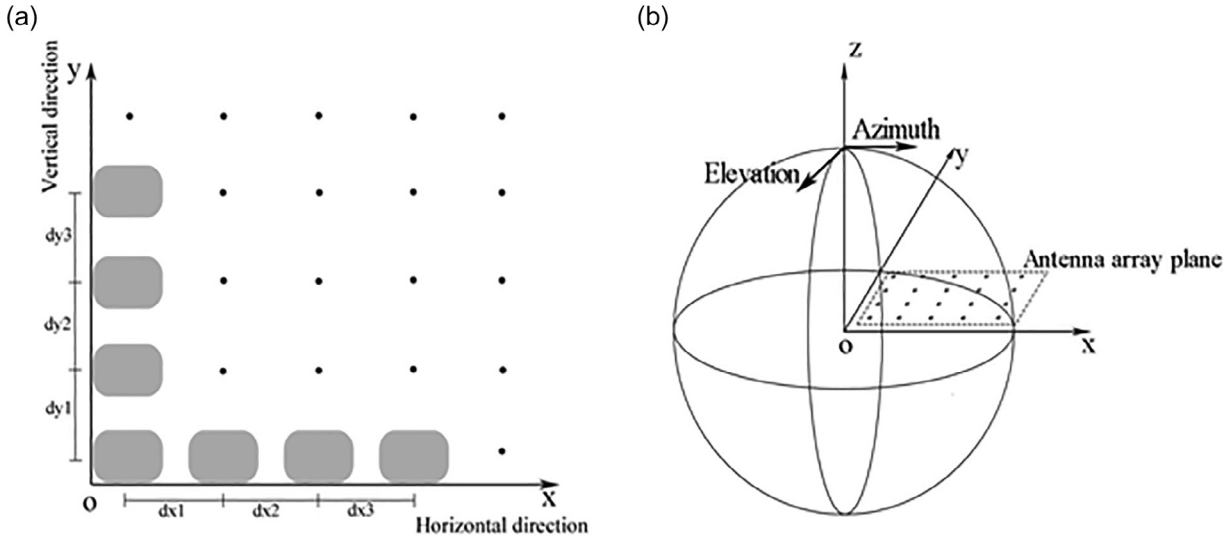

Fig. 2. The spatial distribution of antenna array elements (a – distribution of element in horizontal and vertical directions on the array plane; b – antenna array spherical coordinate systems).

Table 3
Comparison of the SLL suppression at different means (dB).

For a horizontal linear PAA			
Radiation direction	Distance between elements d < λ/2 (dx = 0.47λ)	Non-equidistant positioning of elements	Chebyshev distribution of currents over elements
30°	−11.5	−12	−19
45°	−9.9	−7	−8
60°	−6.4	−1.6	−3
For a vertical linear PAA			
Radiation direction	Distance between elements d < λ/2 (dy = 0.47λ)	Non-equidistant positioning of elements	Chebyshev distribution of currents over elements
30°	−12	−11	−16
45°	−10	−5.8	−9
60°	−8	−3	−5

simulation of 6-element PAA with Chebyshev current distribution is carried out to investigate the SLL; for the horizontal line PAA, dx1 = dx2 = dx3 = dx4 = dx5 = dx = 0.47 λ, radiation in directions of 30°, 45° and 60° from the normal direction was used. Similarly, dy1 = dy2 = dy3 = dy4 = dy5 = dy = 0.47 λ, radiation in directions of 30°, 45° and 60° from the normal direction was used in the study of the vertical line PAA. The simulation results are presented in Table 3.

The simulation results of horizontal PAA width, Chebyshev current distribution on the elements concludes that in the radiation direction of ± 60° from the normal side lobe increased to −3dB and in the radiation direction of ± 45° from normal side lobe increased up to −8 dB. It is acceptable in practice. In the radiation direction of from −30° to 30° relative to the normal side lobe was maximally suppressed to the level of −19 dB. The results are similar for the vertical PAA width Chebyshev current distribution.

The performance comparison of the three methods for the suppression of the SLL is presented in Table 3. The results show that Chebyshev current distribution on the elements reduce significantly the SLL in the radiation direction to ± 60° from the normal. It has a range from −30° to 30° relative to the normal to radiate energy effectively and allows of significance reducing to the SLL (up to −19 dB and −16 dB for horizontal and vertical arrays, respectively).

Linear PAA with Chebyshev currents distribution on the elements both in the horizontal and vertical directions reduces significantly the side lobes and provides a range of scanning beams. Therefore, Chebyshev distribution of the currents on the elements and the distance between elements of 0.47 λ (dx = dy = 20 mm) were chosen for the creation and simulation of flat PAA. The prototyped antenna is shown in Fig. 3.

Simulation of a flat microstrip PAA for emitting the beams

A flat array with 4 × 4 dimension was developed. The number of radiating beams depends on the number group of excitation signals. Superposition of excitation signals was used to radiating several independent beams simultaneously. The direction of radiation (reception) in azimuth and elevation depends on the progressive phase distribution in the excitation signal group in the horizontal (on x-axis) and vertical (on y-axis) directions on the array plane [23]. The weighting coefficients in the superposition of excitation signals corresponded to Chebyshev distribution in the horizontal and vertical directions is investigated to reduce the SLL [17,18]. For the formation of beams superposition, a groups of excitation signals were used, each of them was responsible for the formation of a certain beam.

In the simulation and the calculation, a group of 16 excitation signals for forming a single beam was used. The phase shift in the horizontal direction (on x-axis) was $\Delta\boldsymbol{\alpha}_1$ for the formation of maximum radiation in the direction of azimuth. Additionally, the phase shift in the vertical direction (on y-axis) was $\Delta\boldsymbol{\beta}_1$ for the formation of maximum radiation in the direction of the elevation. The weighting amplitude coefficients in the horizontal and vertical directions corresponded to Chebyshev distribution is 1:3:3:1.

The superposition of two groups of excitation signals was used to form two beams simultaneously: the first group of 16 excitation signals to form a beam in the direction of the azimuth, elevation; the second group of 16 excitation signals to form a beam in the other direction of the azimuth, elevation. The phase shift of the first group in the horizontal direction (on the x-axis) was $\Delta\boldsymbol{\alpha}_1$ for the formation of maximum radiation in the direction of azimuth, the phase shift in the vertical direction (on the y-axis) was $\Delta\boldsymbol{\beta}_1$ for the formation of maximum radiation in the direction of the elevation. For the formation of the second beam in the direction of the azimuth, elevation, the phase shift in the second group of 16 excitation signals was $\Delta\boldsymbol{\alpha}_2$ on the x-axis to form the maximum radiation in the direction of azimuth and $\Delta\boldsymbol{\beta}_2$ on the y-axis to form the maximum radiation in the direction of the elevation. After superposition of excitation signal groups, the signals were weighed with coefficients 1:3:3:1 in the horizontal (on x-axis) and vertical (on y-axis) directions.

By analogy, for the formation of simultaneously independent n beams the superposition of n groups of excitation signals was used. Each of them was responsible for the formation of a certain beam and consisted of 16 excitation signals. After the superposition of excitation signal groups, the signals were weighed with Chebyshev coefficients 1:3:3:1 in the horizontal (on x-axis) and vertical (on y- axis) directions. The superimposed excitation signal on the m-th element of PAA can be summarized as $S_m(t) = x_1(2\pi ft + \boldsymbol{\alpha}_1 + \boldsymbol{\beta}_1) + x_2(2\pi ft + \boldsymbol{\alpha}_2 + \boldsymbol{\beta}_2) + \ldots + x_n(2\pi ft + \boldsymbol{\alpha}_n + \boldsymbol{\beta}_n)$; where m = 1,2,…,16, $x_n(2\pi ft + \boldsymbol{\alpha}_n + \boldsymbol{\beta}_n)$-excitation signal to form a n-th beam in the direction of the elevation and azimuth, f-resonant frequency.

Experimental measurement of the frequency bandwidth of the developed PAA

In order to reduce the electromagnetic mutual coupling between the antenna patches and the feeder lines a structure consisting of seven layers was developed. The seven layers are from top to bottom: antenna patches, dielectric-1 (Arlon AD255 with dielectric permeability ε = 2.55 and thickness of 2.032 mm), ground (copper), a dielectric binder-2 (FR-4 with dielectric permeability ε = 4.34 and thickness of 0.1 mm), ground (copper), dielectric-3 (Rogers 4003 with dielectric permeability ε = 3.55 and thickness of 0.305 mm) and feeder lines (copper). The feeder is connected to the patch through a via hole. The location of the antenna patches and the feeder lines on separate layers allows the reducing of a mutual coupling between them [23–25].

The one port was measured as shown in Fig. 4, and the others were measured in turn. The simulation and measurement results on the 16 ports showed that the PAA operates at frequency band 6.9–7.4 GHz, a central frequency at 7.15 GHz; the resonant frequency of all ports is slightly higher than the values in the simulation; the relative bandwidth at the level of −10 dB is up to 7%.

Feed network of phased antenna array

The old classical pioneer methods for array synthesis are discussed [17–21]. In these classical methods, the analog power dividers and phase shifts are used to realize the required power weights and phase shifts on elements.

A new feeding method is proposed in this paper for the MIMO communication system. The digital beamforming codes are generated in a Field Programmable Gate Array (FPGA) on the digital signal processing (DSP) board. The 16 array elements are fed by 16 transceivers; each transceiver represents a channel in the communication system.

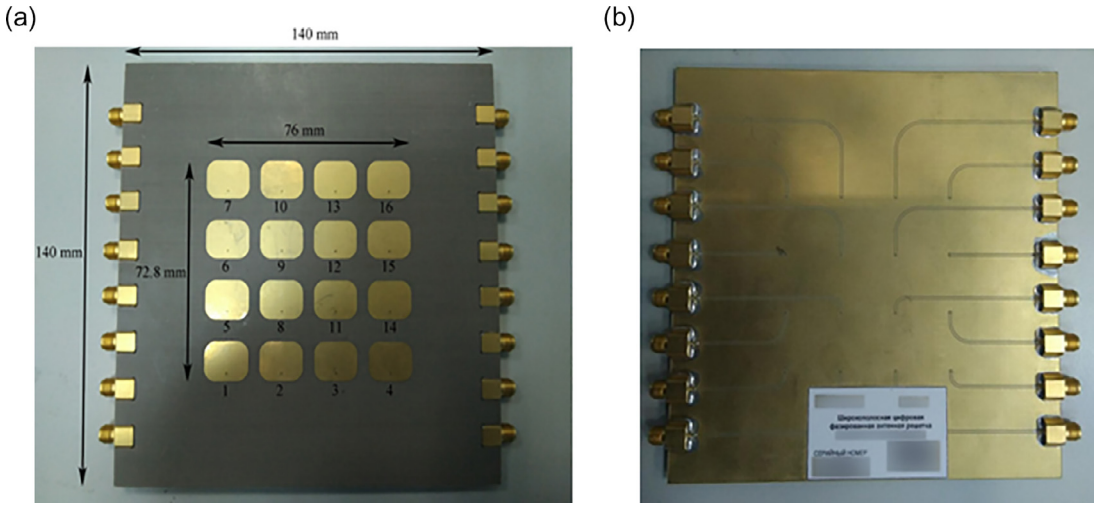

Fig. 3. The top (a) and bottom (b) views of the prototyped antenna array.

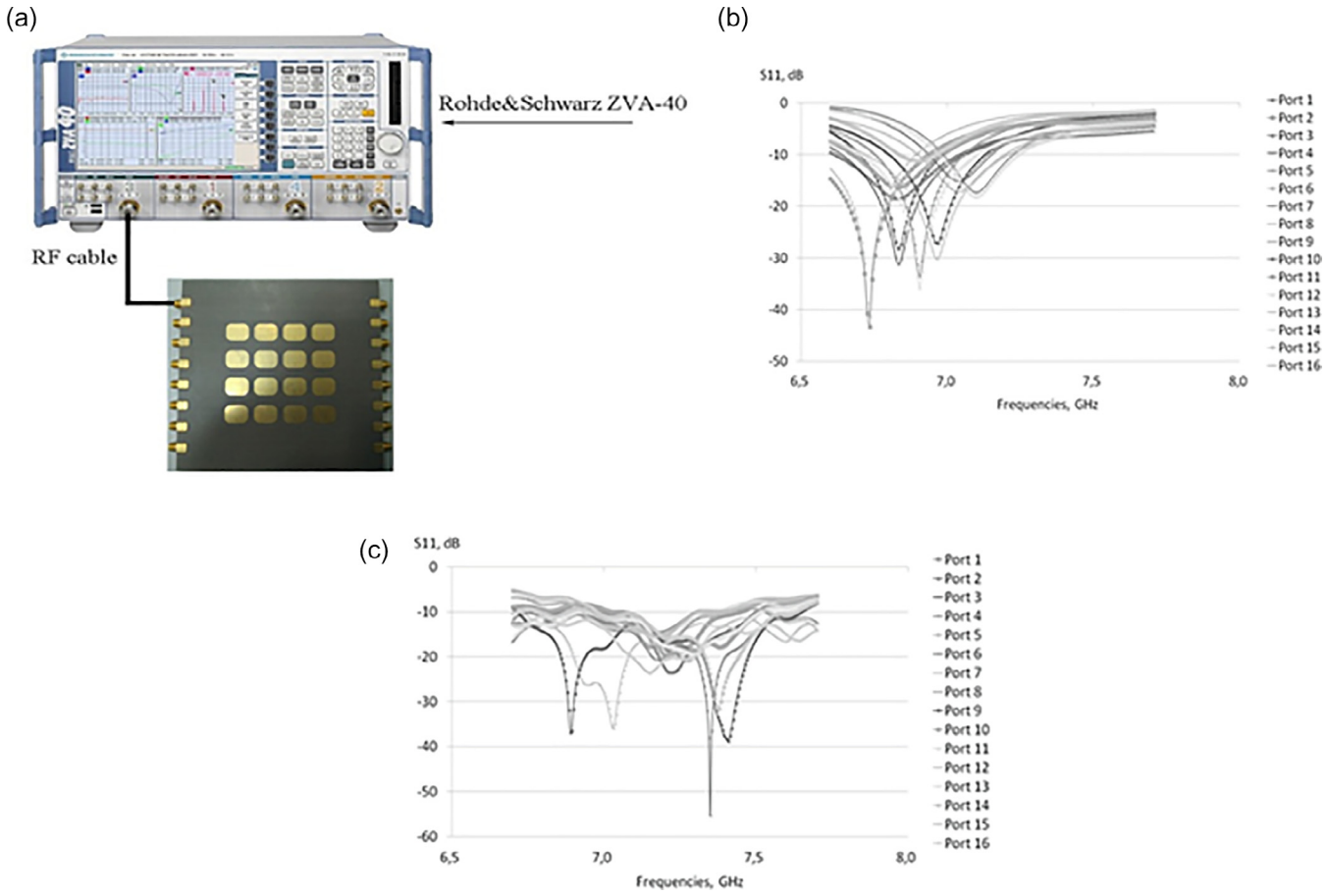

Fig. 4. The result of the simulation and experimental measurement of S11-parameters on all ports (measurement process in (a), simulation results in (b), measuring results in (c)).

The block diagram of feeding system and digital beamforming are shown in Fig. 5. The feeding system is comprised with a control computer, FPGA-boards and 16 transceivers. The beamforming codes are loaded by the computer into the FPGA boards through the JTAG interface in turn; the FPGA-boards formed 16 digital signals, each of which was transmitted to a separate transceiver through the digital interface; each transceiver output was generated superimposed radio frequency(RF) excitation signal and connected to a separate antenna array element. On the m-th array element an superimposed excitation signal is $S_m(t) = x_1(2\pi ft + \boldsymbol{\alpha}_1 + \boldsymbol{\beta}_1) + x_2(2\pi ft + \boldsymbol{\alpha}_2 + \boldsymbol{\beta}_2) + \ldots + x_n(2\pi ft + \boldsymbol{\alpha}_n + \boldsymbol{\beta}_n)$, where $m = 1,2,\ldots,16$; the excitation signal $x_n(2\pi ft + \boldsymbol{\alpha}_n + \boldsymbol{\beta}_n)$ to form the n-th beam, f is the frequency of the excitation signal. In order to simplify the programming, the excitation signal is in cosine form, that is $x_n(2\pi ft) = \cos(2\pi ft)$. On the antenna array plane the horizontal phase distribution vector $\boldsymbol{\alpha}_n$ is used to control the beam pointing in azimuth direction of the n-th beam, and the vertical phase distribution vector $\boldsymbol{\beta}_n$ is used to control the beam pointing in elevation direction of the n-th beam.

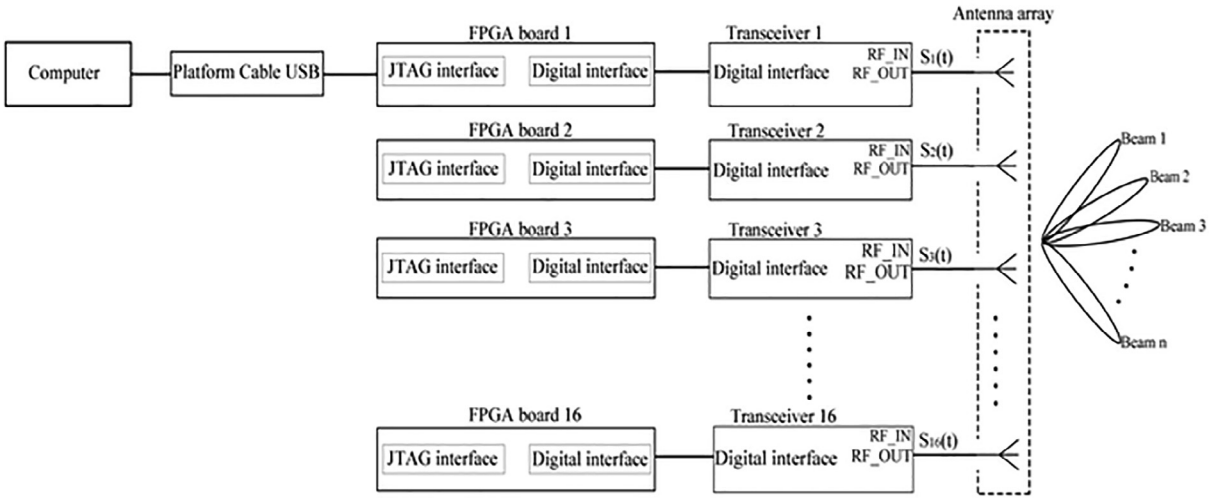

Fig. 5. Block diagram of feeding and beamforming network.

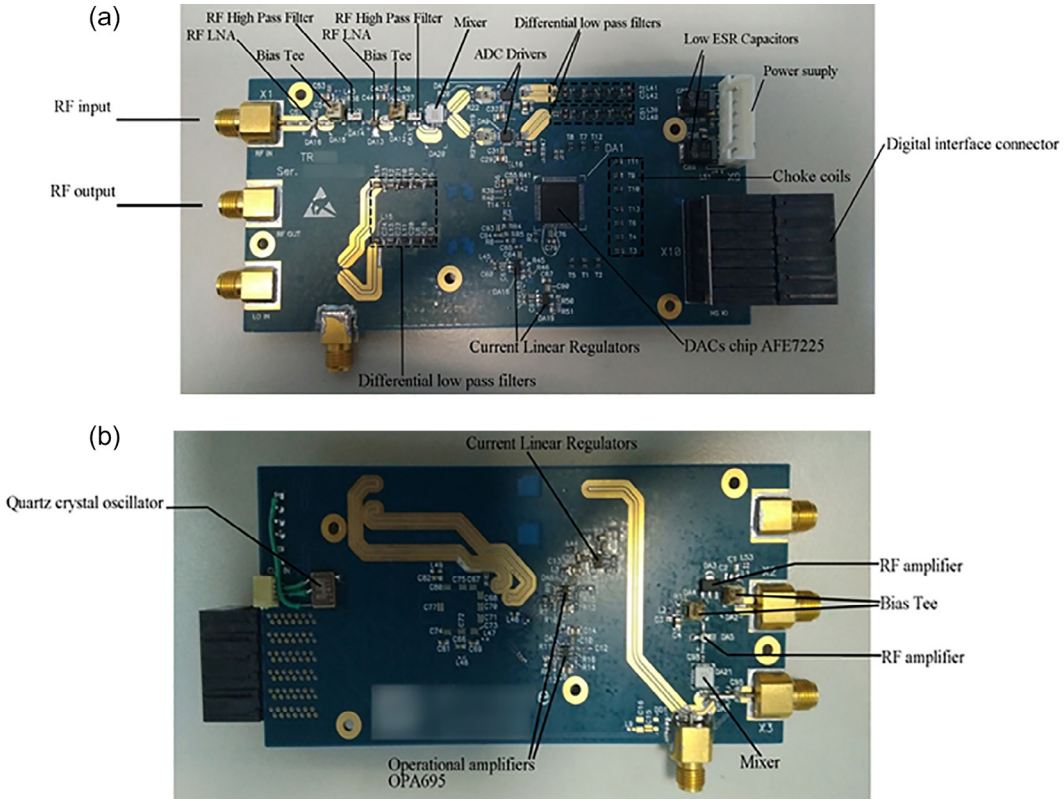

Fig. 6. The top and bottom views of the transceiver (a – top, b – bottom).

In this feeding method, the amplitude weight and phase distribution (α_n, β_n) of each antenna array element's excitation signal $S_m(t)$ are directly realized by digital programming. Therefore, the use of power divider or time-delay systems is avoided. Therefore, the beam scanning can be realized quickly by programming design.

The transceiver performs the functions of digital-analog to conversion (DAC and ADC), converting the frequency between the carrier and zero frequencies, amplification and filtering. It consists of two parts, a transmitter and a receiver. The main components of transceiver are a DAC chip, low frequency amplifiers, L-C low pass filters (LPFs), a quadrature modulator and a demodulator (quadrature mixers), a low-noise RF amplifiers, and RF band-pass filters. The DAC chip (Texas Instruments AFE7225) is used by both transmitter and receiver. The transceiver operates in half duplex mode; transmitter works to generate beams. The receiver digitizes the received target signal and transmits it to the FPGA board as well as background computer for signal processing. The developed transceiver is shown in the Fig. 6. The transceiver operates at the frequency band 4–8 GHz and achieves a maximum transmission speed of 35 Mbit/s in the frequency band 6.8–7.2 GHz. Therefore, antenna resonant frequency is taken at 7 GHz. The size of the transceiver is 130 × 65 × 43 mm. Corresponding to the block diagram in Fig. 5 the feeding setup is shown in Fig. 7. In order to simplify the display of Fig. 7, two transceivers and two FPGA boards are only shown in this paper.

In order to evaluate the developed antenna array with the transceiver and simplify the programming, the two single beams are formed and measured. For a single beam the excitation signal can be simplified as $S_m(t) = x_1(2\pi ft + \alpha_1 + \beta_1) = \cos(2\pi ft + \alpha_1 + \beta_1)$, the direction of a

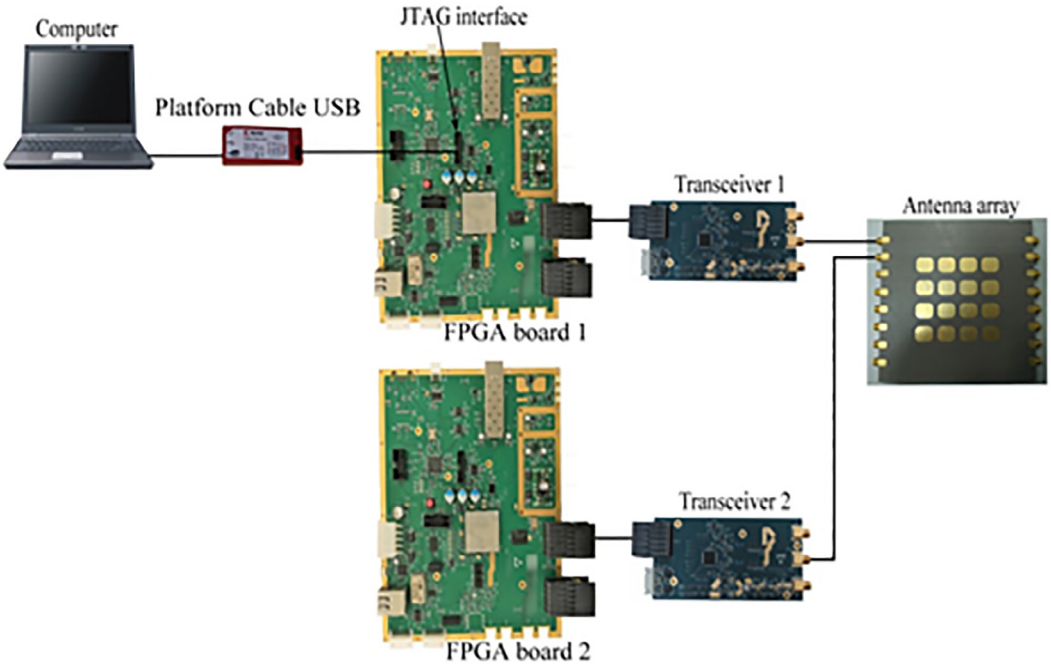

Fig. 7. The block diagram of feeding experimental setup.

Table 4
The amplitude and phase distribution of the excitation signal on the array elements for two single beams.

Direction of beam azimuth = 30°, elevation = 0°																
Element number	1	2	3	4	5	6	7	8	9	10	11	12	13	14	15	16
Amplitude weighting	1	3	3	1	3	3	1	9	9	3	9	9	3	3	3	1
Phase distribution																
α_1	0	86	172	258	0	0	0	86	86	86	172	172	172	258	258	258
β_1 (degrees)	0	0	0	0	0	0	0	0	0	0	0	0	0	0	0	0
Direction of beam azimuth = 0°, elevation = 30°																
Element number	1	2	3	4	5	6	7	8	9	10	11	12	13	14	15	16
Amplitude weighting	1	3	3	1	3	3	1	9	9	3	9	9	3	3	3	1
Phase distribution																
α_1	0	0	0	0	0	0	0	0	0	0	0	0	0	0	0	0
β_1 (degrees)	0	0	0	0	86	172	258	86	172	258	86	172	258	86	172	258

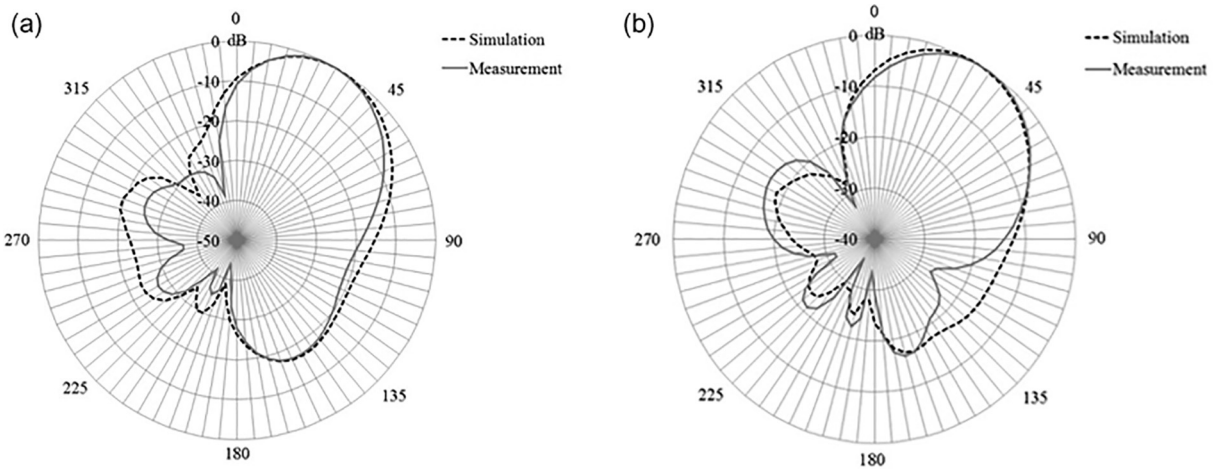

Fig. 8. The patterns of two single beams (a – xz plane, pattern of beam in direction azimuth = 30°, elevation = 0°; b – yz plane, pattern of beam in direction azimuth = 0°, elevation = 30°).

beam with azimuth = 30°and elevation = 0°, the direction of the other beam with azimuth = 0° and elevation = 30°. The array element number and corresponding port are shown in Fig. 3. The amplitude and phase distributions corresponding to the two single beams are presented in the Table 4. The weighting amplitude coefficients corresponded to Chebyshev distribution is to reduce the SLL. In order to generate phase and amplitude distributions of excitation signals in Table 4, the codes for Xilinx FPGA and interface with the transceiver DACs were developed. The radiation patterns of the two single beams are shown in Fig. 8, the SLL is basically consistent with the specified value.

Conclusions

In this paper, a digital technique to realize the fixed amplitude and phase distribution is proposed to generate the beam. Based on this approach, the other types of amplitude and phase distributions on array elements can also be achieved through digital programing. In the future research, the focus will be on the study of using the digital programming to achieve superposition of the signals with dynamic amplitude and phase control in term of generating the multiple independent beams scan. This paper experimentally demonstrates the potential of extracting, processing and identifying the target information through the digital programming.

The shape of an element for building a planar array is selected to providing a wideband approach. Chebyshev current distribution on the elements at the distance of element spacing of the PAA with a value of 0.47λ can maximally suppressed the side lobe level. The number of independent beams is determined by the number of group for the excitation signals at its input ports. The phase shift of each group for the excitation signals in the horizontal and vertical directions in the PAA plane (on the axis OX and OY) determines the direction of the beam. The experimental prototype of an antenna array and transceivers for digital signal processing by an FPGA enables us to digitally form an specified radiation pattern of the beam.

Appendix A. Supplementary material

Supplementary data to this article can be found online at https://doi.org/10.1016/j.rinp.2019.102310.

References

[1] Jensen MA, Wallace JW. A review of antennas and propagation for MIMO wireless communications. IEEE Trans Antennas Propag 2004;52(11):2810–2.

[2] Andersen JB. Array gain and capacity for known random channels with multiple element arrays at both ends. IEEE J Select Areas Commun 2000;18:2172–8.

[3] Wallace JW, Jensen MA, Swindlehurst AL, Jeffs BD. Experimental characterization of the MIMO wireless channel: Data acquisition and analysis. IEEE Trans Wireless Commun 2003;2:335–43.

[4] Molisch AF, Win MZ. MIMO systems with antenna selection. IEEE Microwave Mag 2004;5(1):46–56.

[5] Hechavarria R, Delgado O, Hidalgo A, Espin S, Guamanquispe J. Photothermal technique for measuring thermal conductivity and diffusivity of nanofluids: a new approach. Periodico Tche Quimica 2018;15(29):257–65.

[6] Lienard M, Degauque P, Baudet J, Degardin D. Investigation on MIMO channels in subway tunnels. IEEE J Select Areas Commun 2003;21:332–9.

[7] Zheng L, Tse D. Diversity and multiplexing: A fundamental tradeoff in multiple antenna channels. IEEE Trans Inf Theory 2003;49:1073–96.

[8] Zhang J, Zheng Zh, Zhang Y, Xi J, Zhao X, Gui G. 3D MIMO for 5G NR: several observations from 32 to massive 256 antennas based on channel measurement. IEEE Commun Mag 2018;56(3):62–70.

[9] Lodro MM, Majeed N, Khuwaja AA, Sodhro AH, Greedy S. Statistical channel modelling of 5G mm Wave MIMO wireless communication. In: 2018 international conference on computing, mathematics and engineering technologies; 2018. p. 1–5.

[10] Jilani SF, Alomainy A. Millimetre-wave T-shaped MIMO antenna with defected ground structures for 5G cellular networks. IET Microwaves Antennas Propag 2018;12(5):672–7.

[11] Petrov BM. Electrodynamics and propagation of radio waves. Moscow: Hotline-Telecom; 2007.

[12] Sklyar B. Digital communication. Moscow: Williams Publishing house; 2003.

[13] Slyusar VI. Digital antenna arrays are the future of radiolocation. Electron: NTB 2001;3:42–7.

[14] Slyusar VI. Phased antenna array of Thuraya system. Networks Telecommun 2002;5:54–8.

[15] Geniatulin KA, Nosov VI. Planning of satellite communication systems with zonal service. Vestnik of SibSUTIS 2009;4:11–22.

[16] Zakharov PN, Dudov RA, Mikhailov EV, Korolev AF, Sukhorukov AP. Finite integration technique capabilities for indoor propagation prediction. 2009 Loughborough Antennas & Propagation Conference (LAPC); 2009. p. 369–72.

[17] Siakavara K, Chrysomallis M, Fernandez Jambrina JL, Sahalos JN. An antenna array synthesis technique by the help of Chebyshev polynomials. Electr Eng 1989;72(6):435–41.

[18] Elliott RS. Synthesis of rectangular planar arrays for sum patterns with ring side lobes of arbitrary topography. Radio Sci 1977;12(5):653–7.

[19] Goto N. A synthesis of array antennas for high directivity and low sidelobes. IEEE Trans Antennas Propag 1972;20(4):427–31.

[20] Laxpati S. Planar array synthesis with prescribed pattern nulls. IEEE Trans Antennas Propag 1982;30(6):1176–83.

[21] Freese J, Jakoby R, Blocher H-L, Wenger J. Synthesis of microstrip series-fed patch arrays for 77 GHz-sensor applications. Asia-Pacific Microwave Conference Proceedings 2000.

[22] Vendik OG, Parnes MD. Introduction to the Theory of electronically steerable antennas. Moscow: Radio i Svyaz; 2001.

[23] Goming Lu, Zakharov PN, Sukhorukov AP. Simulation of low-sidelobe phased antenna array with circular polarization. Moscow University Physics Bulletin. Series 3. Phys Astron 2013;6:3–7.

[24] Fenn AJ, Temme DH, Delaney WP, Courtney WE. The development of phased-array radar technology. Lincoln Laboratory J 2000;12(2):320–40.

[25] Daryoush AS. Digitally beamformed multibeam phased array antennas for future communication satellites. 2008 IEEE Radio and Wireless Symposium; 2008. p. 831–4.